HHS Public Access

Author manuscript

J Control Release. Author manuscript; available in PMC 2016 December 10.

Published in final edited form as:

J Control Release. 2015 December 10; 219: 536–547. doi:10.1016/j.jconrel.2015.10.006.

Control of Polymeric Nanoparticle Size to Improve Therapeutic Delivery

John W. Hickey[1,2,3,4], **Jose Luis Santos**[2,4,5], **John-Michael Williford**[1,2,4], and **Hai-Quan Mao**[2,4,5,6]

[1]Department of Biomedical Engineering, Johns Hopkins School of Medicine, Baltimore, Maryland 21205

[2]Institute for NanoBioTechnology, Johns Hopkins University, Baltimore, Maryland 21218

[3]Institute for Cell Engineering, Johns Hopkins School of Medicine, Baltimore, Maryland 21205

[4]Translational Tissue Engineering Center, Johns Hopkins School of Medicine, Baltimore, MD, 21287

[5]Department of Materials Science and Engineering, Johns Hopkins University, Baltimore, MD, 21218

[6]Whitaker Biomedical Engineering Institute, Johns Hopkins University, Baltimore, MD 21218

Abstract

As nanoparticle (NP)-mediated drug delivery research continues to expand, understanding parameters that govern NP interactions with the biological environment becomes paramount. The principles identified from the study of these parameters can be used to engineer new NPs, impart unique functionalities, identify novel utilities, and improve the clinical translation of NP formulations. One key design parameter is NP size. New methods have been developed to produce NPs with increased control of NP size between 10 to 200 nm, a size range most relevant to physical and biochemical targeting through both intravascular and site-specific deliveries. Three notable techniques best suited for generating polymeric NPs with narrow size distributions are highlighted in this review: self-assembly, microfluidics-based preparation, and flash nanoprecipitation. Furthermore, the effect of NP size on the biological fate and transport properties at the molecular scale (protein-NP interactions) and the tissue and systemic scale (convective and diffusive transport of NPs) are analyzed here. These analyses underscore the importance of NP size control in considering clinical translation and assessment of therapeutic outcomes of NP delivery vehicles.

Graphical Abstracts

*Correspondence should be addressed to Hai-Quan Mao at 3400 N. Charles St., 113 Maryland Hall, Johns Hopkins University, Baltimore, MD 21218; Tel: 410-516-8792, Fax: 410-516-5293, hmao@jhu.edu.

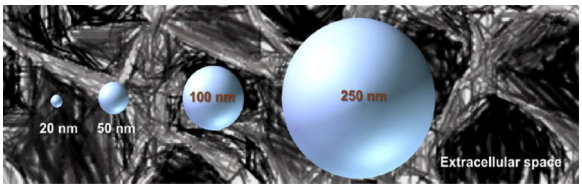

Keywords

size control; polymeric nanoparticles; nanomedicine; drug delivery

1. Introduction

Nanoparticles (NPs) continue to be investigated for their potential to improve existing therapies and to develop novel therapies. At a length scale of less than 200 nm, NPs with encapsulated therapeutics can be injected intravascularly without the concerns of embolization; they have the potential to permeate and traffic through different tissues, can bind to cell surface receptors, enter target cells for intracellular delivery of the cargos, and influence the intracellular tracking pathways. Due to these unique characteristics, a multitude of applications have been identified for NP-mediated delivery. Examples include targeted delivery to localized and metastatic cancers, cell- or tissue-specific delivery of imaging agents for disease diagnosis, DNA- and RNA-based gene delivery, and prophylactic treatment of infectious diseases. The expanding range of applications in turn has motivated further development of NP formation techniques with more precise control over particle geometry and physicochemical properties.

Despite the progress made, the effect of NP size on their transport properties and delivery efficiency remains poorly understood. This is largely due to the limited number of methods to generate NPs with well-controlled size and high degree of uniformity. Recent studies have shown that NP size plays a critical role in modulating their interactions with the biological milieu following administration, ranging from molecular binding and NP surface-modification, to cell-NP binding, internalization, and intracellular trafficking, to vascular distribution, extravasation, and tissue diffusion, thereby dictating the overall delivery efficiency. These findings have highlighted the need to develop methods for controlling the size and uniformity of NPs prepared from a wide range of materials. Here we review the principles, materials choices, cargo loading capacity, and unique features of several major polymeric NP preparation methods that allow size control, and contrast their advantages and disadvantages. Moreover, the effect of NP size on biological interactions at the molecular, tissue, and systemic levels are highlighted.

2. Methods to Generate NPs with Controlled Size

Controlling NP size and size distribution through assembly of polymeric building blocks and therapeutic agents requires understanding of molecular forces governing NP formation. Physicochemical properties of the components, phase transition kinetics and fluid dynamics, and manufacture processes all contribute to NP size control. Here we review key parameters

for controlled NP assembly and highlight techniques that promote control over NP size and distribution.

Generating nanoparticles with narrow size distribution is critical to investigating NP-size effects on their transport properties, biological activity, and therapeutic efficiency [1]. NP size and polydispersity are generally measured by a combination of methods including transmission electron microscopy, atomic force microscopy, fluorescence correlation spectroscopy, analytical ultracentrifugation, dynamic light scattering, and particle diffusivity [2–4]. It is worth noting that reporting results from a combination of these methods will facilitate meta-analyses of NP-size related studies across different platforms.

2.1 Molecular Interactions and Parameters Governing NP Formation

Self-assembly of polymeric building blocks into NPs with well-defined physicochemical properties—size, shape, surface chemistry, and functionality—has been widely explored as a means to develop efficient drug delivery devices and diagnostic tools. The spontaneous self-assembly of these macromolecules into polymeric nanostructures generally relies on secondary intermolecular interactions including hydrophobic-hydrophobic interactions, hydrogen bonding, electrostatic interactions, stereocomplexation, π-π stacking, and host-guest interactions [5–8]. Through modulation of chemical building blocks, one can alter self-assembly processes and control the structure and physicochemical properties of the assembled particles [9]. In addition, polymers with narrow molecular weight distributions could yield NPs with lower size heterogeneity.

Other than control of physicochemical properties of the polymers, the preparation method of polymeric NPs plays a crucial role in preparing NPs with the desired size and properties. The formulation of polymeric nanoparticles of various sizes, shapes and narrow distribution is the result of a complex equilibrium between the chemical identity of the building blocks and the processing conditions including mixing dynamics and solvent conditions.

A number of recent reviews have highlighted the use of batch-mode processing methods (slow precipitation, dialysis, emulsion, etc.) to prepare various polymer NP formulations for therapeutic delivery [10–12]. Here we will focus on newer methods with better control over particle size and higher degrees of reproducibility, scalability, and capacity. Table 1 summarizes the major methods for polymeric NP preparation, their unique features, suitable polymer carriers for each methods, and possible therapeutics that can be packaged into the NPs.

2.2 Flow-based Preparation Methods

Flow-based preparation methods rely on utilizing the ability to control the fluidics or mixing dynamics of the NP forming polymer solutions. This may include combination of agents to initiate polymerization, chemical reactions, or aggregation via quick exchange of solvents. Typically this is accomplished within the context of mixing and has been controlled in microfluidic or flash nanoprecipitation devices. The mixing that occurs within these devices happens on the order of a few milliseconds and provides the needed control over efficient and homogeneous mass transfer to achieve monodisperse NP formulations.

2.2.1 Microfluidic Devices—Microfluidic devices are a versatile platform that can be used to prepare various types of polymeric nanoparticles. One advantage to using microfluidics is that it enables precise liquid handling (nanoliter to picoliter scale) within microchannels of dimensions between a few tens to hundreds of microns. This both creates a high surface-to-volume ratio and enables rapid and controlled micromixing ensuring efficient and homogeneous mass transfer [13]. In addition, continuous in-line production mitigates batch-to-batch variability, an important quality factor for scale-up and commercialization. In comparison to conventional batch-mode preparation methods, microfluidic devices offer superior control over NP yield and physicochemical properties [14, 15].

On a microfluidic device, NP size can be readily tuned by adjusting the flow rate (mixing times), magnitude of the solvent jump, solvent polarity, concentration, and composition of the polymers. For instance, the Karnik and Farokhzad groups have developed several microfluidic platforms capable of generating size-tunable polyethylene glycol-*b*-poly(lactic-co-glycolic acid) (PEG-*b*-PLGA) NPs with narrower size distribution, higher drug loading capacity, and improved batch-to-batch consistency when compared with those prepared from a conventional precipitation method [16, 17] (Figure 1a). Particle size was tuned in the range of 30–200 nm by altering mixing time of precursors, the flow ratio, concentration, or molecular weights of the polymer. Such platforms offer great versatility and have been used to prepare PEG-*b*-PLGA NPs of 100 nm to co-deliver drugs with distinct solubility profiles and modes of action (cisplatin and docetaxel/irinotecan) to prostate cancer cells [18, 19].

In addition, microfluidic platforms can be designed to enable high-throughput engineering of hundreds of NP formulations by on-line manipulation of process parameters. The systems are designed to allow high precision automated metering, dilution, and mixing of the molecular components, resulting in a combinatorial library of NPs with broad structural and functional properties in only a couple of hours. This approach reduces the time needed to select an optimal formulation as well as the cost associated with reagents and labor. Moreover, this approach expedites the discovery of optimal NP formulations to be used first in clinical trials and accelerate the development of effective polymer NP therapeutics for in human use [20, 21].

Although microfluidic devices offer many beneficial control parameters, there are a few issues to consider in working with microfluidic devices when producing polymeric NPs. Microfluidic devices can be made in several geometries and are typically fabricated in polydimethylsiloxane (PDMS), polymethyl methacrylate, polycarbonate, and polyurethane [22–24]. Some of these materials are very sensitive to organic solvents leading to swelling, deposition of bioactive agents, or even aggregation of polymers (e.g. PLGA) on channel walls often resulting in channel clogging. Swelling of microchannels alters the characteristic laminar flow patterns and increases the formation of by-products [25]. Coating the surface of microchannels with chemically resistant materials, which is rather a time-consuming and expensive process, can solve this common bottleneck. Better alternatives have therefore been developed and they include the fabrication of microfluidic devices with glass and stainless steel, which are chemically resistant to virtually any chemical that is used in processing polymer nanoparticles [26, 27]. Optimization of microfluidic devices on all

fronts has also lead to development of microfluidic platforms capable of producing up to 250 g of polymer nanoparticles/day with excellent control over particle size and size distributions (PDI < 0.1) [26].

2.2.2 Flash Nanoprecipitation—Flash nanoprecipitation (FNP) is a simple, continuous, and scalable process that allows the production of block copolymer NPs. This process uses rapid micromixing (on the order of millisecond) to establish homogeneous supersaturation conditions and controlled precipitation of hydrophobic solutes (organic or inorganic) along with block copolymer self-assembly [38, 50]. Rapid mixing conditions are achieved using confined precipitation geometries with two (e.g. in a confined impinging jet mixer, CIJ mixer) or more impinging fluid streams (e.g. in multi-inlet vortex mixer, MIVM) (Figure 1b). In both cases, the organic stream, which contains the active solute and the stabilizing block copolymer, and the antisolvent streams are brought together into a confined cavity to initiate homogenous and rapid precipitation of all components to produce NPs that are sterically stabilized by the hydrophilic component of the copolymer [40]. NPs with narrow (PDI < 0.15) and tunable size distributions from 30 to 300 nm can be readily obtained by fine-tuning the kinetics of micromixing (flow rates and mixer geometry), solute nucleation and growth, and block copolymer structure [43].

The versatility offered by FNP has been applied to the production of multifunctional NPs and composite NPs comprised of inorganic and organic cores with encapsulated therapeutic and imaging agents [34–36, 42, 44]. Furthermore, FNP enables the preparation of NPs with well-defined density of targeting ligands by simply co-mixing functionalized and non-functionalized block copolymer chains [37, 39]. This technique has shown great efficiency for encapsulating hydrophobic cargos using block copolymers with the matching solvent systems. In addition, this method has recently been used to generate more complex polymer NPs with Janus or patchy structures [41].

2.3 Template-assisted Preparation Methods

2.3.1 Layer-by-layer (LbL) self-assembly—LBL self-assembly using size-controlled core nanoparticles (gold, silica, calcium phosphate nancrystals and PLGA nanoparticles) on which layers of polymers or biological molecules (DNA or RNA) are sequentially deposited following core removal is another approach to prepare polymer NP with well defined size (40 – 500 nm) and therapeutic cargo loading (Figure 1c) [29, 33, 51]. In addition, polymer NPs of different shape can be readily prepared by using core nanoparticles of various geometries. A major bottleneck of LBL assembly on nano-sized templates is the need of a centrifugation step to remove excess of polymers during the assembly process. Sequential washing/centrifugation cycles might lead to significant aggregation of nanoparticles thus making automation, scale-up and low batch-to-batch variability challenging to achieve. To address current challenges associated with scale up of LBL process, the Caruso group has develop a new fluidic setup for LBL self assembly of polymer NPs resembling closed-loop systems used in industry for the formulation of biotherapeutics [52]. The fluidic setup incorporates a tangential flow filtration (TFF) module that enables the removal of excess polymer used during each layering step. Depending on the pore size of the TFF membrane module, core template and average molecular weight of polymers used, NPs of size ranging

50 – 500 nm can be engineered with higher reproducibility with improved mechanical performance. In addition, the system allows for high throughput screening and is amenable for scale up.

2.3.2 PRINT Technology—Particle Replication In Nowetting Templates (PRINT) is a versatile "top-down" method that has been employed in the fabrication of polymeric NPs. PRINT technology makes use of highly fluorinated perfluoropolyether (PFPE) elastomer as a mold, which has a very low surface energy compared to other materials enabling easy harvest of objects [48]. It offers excellent orthogonal control over particle size; shape, chemical composition, and processing conditions are mild enough to fabricate therapeutic NPs containing bioactive agents (DNA, siRNA, and proteins) [25, 31, 48]. Highly monodisperse polymer NPs with sizes ranging 100–500 nm and shapes including spheres, cylinders, disks, cones and Janus particles can be fabricated with high uniformity and in a highly scalable manner [31, 49].

2.4 Scalability and Reproducibility of the Production Methods

In general, the LbL method is a versatile approach to prepare NPs of controllable size, surface properties and capability to deliver both small molecule drugs and electrostatically charged biologics. Recent efforts in the development of scalable methods will eventually ensure its potential for large-scale production [31, 32]. The microfluidic approach offers excellent uniformity because it provides control over mixing and diffusion at the nano-picoliter scale. However, the concern of scalability makes them less suitable for mass production of such particles. The FNP method can overcome this limitation, although it is applicable to a selected group of copolymers and requires solvent exchange to remove the organic solvents used during NP production. Future effort in developing new methods for controlling NP size will likely focus on improving scalability and reproducibility in addition to refining uniformity of the process, thus making it translatable to the manufacturing and clinical testing stages.

3. Molecular-scale Interactions Influence Contextual NP Size

Despite the ability to produce NPs with narrow size distributions, once administered *in vivo*, many additional factors contribute to the actual size in their microenvironment *in vivo*, or "ntextual size"of the NPs. This includes NP aggregation and degradation, NP surface stabilization by proteins after administration, NP destabilization, and NP flexibility. We present how NP size contributes and is influenced by these forces, and how to minimize unwanted effects to maintain NP size.

3.1 Particle Aggregation and Degradation

Though forming smaller particles leads to many beneficial biological properties, smaller particles have a higher free surface energy related to the equation $\Delta_{EX}G = \gamma_{s/l} \cdot \Delta A$ where $\Delta_{EX}G$ is the Gibb's free energy contributed by surface tension, ΔA is the surface area created, and $\gamma_{s/l}$ is the interfacial tension [53]. As particle curvature increases with decreasing size this increases the interfacial tension experienced by the NP. The complex interactions at this interface are governed by a number of forces including electrostatic,

solvation, and Van der Waals forces, which cause NPs to reduce the interfacial tension and thus the free energy of the system [54]. One way NPs minimize this tension is binding to other NPs. There are many techniques to minimize NP aggregation with various advantages and disadvantages for each method [55]. One approach is to sterically hinder NP aggregation in the addition of an inert polymer. Additionally, NPs can be charged electrostatically to prevent further NP-NP interactions, though this effect will often be reduced in the case of electrolyte-filled biological solutions.

Just as size creates further issues for NP stability and aggregation, it also affects NP degradation. For polymer NPs, the high surface area to volume ratio contributes to a larger portion of the material exposed to media and enzymes. This generally increases degradation rates for decreasing NP size. Furthermore, polymer composition also plays a role if degradation products are autocatalytic such as lactic acid and glycolic acid from PLGA [2, 56]. Therefore material choice and, more specifically, molecular weight, chemical structure, glass-transition temperature, degradation products, and crystallinity will be important parameters to optimize when considering NP stability and degradation.

3.2 Corona Formation

Even with NP stabilization techniques to prevent aggregation, NPs will also reduce free energy by interacting with proteins in the biological milieu. Therefore, protein coating could significantly influence the contextual size and the physiological fate of NPs (Figure 2a). NPs with higher interfacial free energy in biological media have a higher tendency to attract serum protein components to minimize surface tension. Protein coronas are formed within 30 seconds of contact with serum and can increase NP-apparent volume by 8-fold in just 10 minutes, leading to aggregation at later time points [57]. Furthermore, NP size alone has been shown to affect protein corona compositions and has been attributed to the curvature of NPs [58, 59]. Consequently, one implication of protein corona formation is that NP sizes should be measured while in a plasma or cell culture media for the duration of anticipated biological residence times. This will aid in more accurately identifying true size-dependent NP properties.

3.2.1 Preventing Corona Formation—Most often in therapeutic applications, researchers have not been concerned about the effect of protein corona on NP size, focusing instead on NP clearance. As specific proteins adsorb to NPs, such as complement component C3, this leads to increased macrophage uptake, decreased NP targeting, and decreased therapeutic efficiency. Protein corona formation is dependent on many of the same properties that effect NP aggregation: NP size and curvature, hydrophobicity, and surface charge. One common approach to minimize protein absorption and uptake by the mononuclear phagocyte system [60] is the grafting of polyethylene glycol (PEG) on the NP surface. PEG is highly hydrophilic and creates a protective water corona through hydrogen bonding [61]. However, even at high PEG density not all NP protein absorption is prevented [59]. NP size also affects the achievable PEG density. As NP size decreases, the curvature of the NP increases and creates more steric interactions of PEG-like surface-protecting molecules. This decreases the amount of PEG able to be grafted on the surface, limiting protection to protein components.

In many therapeutic applications, NPs are functionalized with cell or tissue-specific protein, peptide, apatamer, or other types of ligands. In these cases, the ability to maximize PEG density or other surface modification schemes is limited. As a result, the non-specific protein coating on NPs may mask functional ligands and decrease targeting efficiency [62]. Therefore, it is important to optimize NP ligand density and configuration. Swami *et al*. recently demonstrated the importance of both characterizing NP size in a biological context and optimizing surface ligand concentration to minimize protein surface absorption (Figure 2b) [63]. When bone-targeting alendronate ligand concentration was above 20% on NP surface, particle size increased from 200 nm to 300 nm when incubated with serum-containing medium. On the other hand, when ligand concentration was lower than 20%, NP size remained unchanged. Such information proves to be useful for NP optimization to achieve efficient bone targeting.

3.2.2 Utilizing Corona Formation—Protein corona formation can be taken advantage of as a NP surface modification approach. By pre-incubating NPs with specific plasma or biological fluids under controlled conditions, it pre-modifies the NPs with a “beneficial” protein corona and results in more predictable NP formulations that prevent further aggregation and exhibit higher colloidal stability *in vivo* [64]. This initial shield layer remains relatively intact, as Tenzer *et al*. demonstrated that only the quantity of the protein corona, but not the composition, changed over time [57]. A caveat is that *in vitro* opsinization as a NP modification strategy could also increase cellular uptake, thus reducing circulation time and potentially masking important functional ligands on the surface of NPs [65, 66]. A more sophisticated approach involves pre-coating NPs with specific proteins native to endogenous cells such as CD47 or “self” peptides designed from anti-phagocytic “self” markers to increase circulation time and inhibit NP-internalization [67]. Alternatively, NPs have even been coated with cell membrane of with red blood cell membranes such that the biodegradable particles are disguised from phagocytic cells, leading to extended circulation time [68]. Accordingly, control over adsorption from “self” proteins *versus* serum proteins need to be balanced depending on what level of cellular interaction and final therapeutic destination of the NPs.

3.3 Dissociation and Particle Disassembly

In addition to increasing the size of NPs, incubation with biological media may decrease particle size by destabilization. This is especially true when forming NP micelles or liposomes, where polymer chains may not be covalently crosslinked [69]. Liu *et al*. recently demonstrated the importance of this phenomena in forming amphipathic micelles (15 – 20 nm) through conjugating protein antigen or adjuvant to a lipid moiety [70]. When injected subcutaneously at a high concentration, these micelles dissociated and the released amphipathic molecules associated with albumin and were transported to the local draining lymph nodes (LNs) by this albumin-mediated mechanism rather than by micelle-mediated delivery, even though these micelles were stable at low concentration. The destabilized micelles demonstrated more efficient LN-transport and retention than stabilized micelles at the similar size range. Understanding NP stability in biological context is critical to the development of efficient antigen delivery system and other therapeutic NPs.

3.4 NP Stiffness

Another parameter dependent on molecular scale interactions that can influence the contextual size and shape of NPs is the flexibility of the NPs. For “softer” NPs, deformation allows passage across biological boundaries such as capillary walls, extracellular matrix (ECM), etc., that are smaller than the hydrodynamic size of the NPs [71]. Thus, the change in functional dimensions of the NPs results in different physiological responses and potentially different biodistribution than that of the same-sized “stiffer” NPs, which do not easily deform due to local pressure difference or shear (Figure 2c) [72]. Surface coatings with different conformations could also change the surface flexibility and contextual size of the NPs. For example, Ogawa *et al*. showed that lysine dendrimer-grafted NPs underwent faster renal clearance even though the hydrodynamic size of the NPs were nearly 15 nm, whereas poly(amidoamine) dendrimer-grafted NPs of a similar size did not. This difference in renal clearance was attributed to the higher flexibility of the lysine dendrimer grafts on NPs, which influenced pharmacokinetics of the dendrimer-modified MRI contrast agent [73]. Therefore, molecular flexibility is an important consideration when comparing size-dependent transport properties of different NP formulations.

4. Size of NPs Influences Their Biodistribution

Tissue factors, such as shear stress from fluidic flow in the blood stream and local changes of interstitial pressure, are exerted on NPs and cause NP movement. NP size influences the capability for NPs to navigate through extracellular matrices and fenestrated tissue *via* fluidic networks. However, the structure and transport properties of different tissues vary greatly. In this context, route of administration is highly relevant in defining NP transport kinetics and delivery efficiency. Common modes of administration of NPs include oral, intravenous (i.v.), subcutaneous (s.c), intradermal (i.d.), intramuscular, nasal, and pulmonary injections, each with corresponding applications and unique features [45, 74–76]. Here we discuss the effect of NP size on biodistribution by the most commonly used routes for delivery of NPs: intravenous injection, tissue-based injection, and mucosal administration.

4.1 Intravenous Injection

Among administration routes, intravenous administration is the most frequently used for targeted delivery of NPs. When NPs are injected intravenously, they circulate throughout the entire body. NPs escape the circulatory system to other tissues by endocytosis, shear forces, or passive diffusion through fenestrations in the capillary network. NPs less than 6 nm are largely cleared by the kidney, whereas those larger than 6 nm are cleared by the liver; furthermore, particles larger than 200 nm are captured within the spleen [77, 78]. These organs comprise major sources of the mononuclear phagocyte system (MPS) [60], and the ability to evade MPS clearance often correlates to increased NP circulation time. A prolonged NP circulation allows for more time for selective delivery to a specific diseased tissue through active targeting, thus improving therapeutic outcomes.

4.1.1 NP Size and the Enhanced Permeability and Retention (EPR) Effect—One targeted site through i.v. injection involves the treatment of solid tumors by harnessing the EPR effect, where NPs injected systemically are able to escape through the leaky

vasculature of solid tumor tissue. The EPR effect provides an important case study for regulating NP transport by controlling NP size (Figure 3a), as it occurs when there is limited lymphatic drainage of the tumor environment and leaky tumor vasculature. The EPR effect is generally limited to NPs between 30 and 200 nm that are able to escape circulation through fenestrations in the capillary network of the tumor tissue [79, 80]. One example of a study that probed further NP size-dependent accumulations in tumors with the EPR effect used boronic acid-rich bovine serum albumin NPs of 70, 110, and 150 nm [81]. The 110 nm NPs had the highest tumor/liver ratio, followed by 150 nm and 70 nm NP respectively. However, beyond the extravasation step, NP trafficking through ECM may be influenced by NP size in a different manner. When PEG-*b*-poly(γ-benzyl L-glutamate) (PEG-*b*-PBLG) NPs were given i.v. in a mouse metastatic cancer model, both the 30-nm and 70-nm PEG-*b*-PBLG micelles, as well as the 80-nm Doxil NPs, were able to accumulate around the tumor vasculature; however, only the 30-nm PEG-*b*-PBLG micelles were able to penetrate into the tumor tissue, resulting in a higher level of overall accumulation (Figure 3b) [82].

4.1.2 Factors to Consider in NP-size EPR Studies—These results suggest the importance for choosing both the size and potentially the disease model in studying the NP EPR phenomenon. Even within leaky tumor models, NP accumulation is limited because of the poor lymphatic drainage from the tumor microenvironment, creating high interstitial pressure within the tumor. Tumor heterogeneity, animal strain, and other disease models contribute to a varied NP size-dependent distribution than that manifested by the EPR effect (Figure 3c). For example, tumors are hypovascular or hypopermeable; they do not exhibit the same size-dependent NP accumulation. PEG-*b*-PBLG copolymer and poly(glutamic acid) NPs were formed with diameters of 30, 50, 70, and 110 nm with similar drug encapsulation concentrations and zeta potentials [83]. Within a leaky tumor model all NPs exhibited similar therapeutic results; however, within a low permeability tumor model, the 30-nm NPs exhibited the highest therapeutic benefit followed by 50-nm NPs. The 70- and 110-nm NPs showed no greater therapeutic advantage than control saline treatment. However, with addition of transforming growth factor beta (TGF-β) to increase the permeability of the hypovascular tumor, all NPs displayed similar penetration depths and mediated similar therapeutic outcomes. Therefore, both the optimal circulating size and penetrating size should be taken into account when designing therapeutic NPs administered *via* i.v. injection.

4.2 Tissue-based Injection

A tissue-based injection is frequently used as an administration route for vaccines, more delicate drugs such as protein drugs, and slow release of a drug as a bolus. When NPs are given through a tissue-based injection, they immediately encounter the ECM. Unlike i.v. injection, tissue-injected NPs do not encounter high fluidic flow rates, and transport of the NPs is based on diffusive properties, the composition of the ECM, lymphatic drainage flow rate, and cellular uptake rate. The size of the spaces created by various compositions and concentrations of filamentous proteins in the ECM acts as a resistance to both convective and diffusive transport of particles [84]. This is proposed to be a major factor influencing NP transport to the target tissue.

42.1 Subcutaneous Injection—One targeted site of tissue-based injections is the lymph nodes (LNs). Targeting the LNs with NPs has major implications in effective delivery of vaccines and immunotherapies for diagnosis and treatment of metastatic cancers. LN-targeted delivery *via* s.c. injection relies on transport of NPs through lymphatic flow (Figure 4a). NPs travel *via* lymphatic flow with interstitial fluid through the ECM to collecting lymphatic vessels, which drain to local LNs.

Primary studies demonstrated that the size of antigen-conjugated, polystyrene NPs of 40 – 50 nm showed the highest accumulation within murine draining LN (dLN) when compared to larger, micron-sized particles and smaller 20-nm NPs [85]. This finding agrees well with the study using biodegradable poly(D,L-lactide-co-glycolic acid) (PLGA)-based NPs, comparing 50-, 100-, and 200-nm NPs for lymphatic transport in a rat model. Results showed that the uptake and LN retention was the highest with 50-nm NPs and decreased with an increased size of the NPs [86], which is similar to studies done with liposomes [87]. Recent studies conducted in porcine models showed that 50-nm polymeric NPs effectively traveled to the LNs nearly 24 cm away, while 120-nm NPs did not [88, 89].

4.2.2 Intradermal Injection—Intradermal (i.d.) injections are often used as a method of vaccination since the dermis is a site with many resident APCs. Similar to s.c. injections, NPs not internalized by resident APCs and local tissue cells also traffic to LNs. NP size is an important factor influencing the delivery efficiency, and similar results to s.c. injections have been observed. Antigen-conjugated polystyrene NPs with a diameter of 40 – 50 nm were injected intradermally and stimulated a higher level of antibody response compared to NPs larger than 100 nm [85]. The smaller NPs traveled more efficiently to the local dLNs, which increased the delivery efficiency of antigen to the APCs. Moreover, intradermally injected 20-nm pluronic-stabilized polypropylene sulfide (PPS) NPs traveled more efficiently through the interstitium to murine dLNs, and were retained longer than 45- and 100-nm NPs [90, 91], whereas the 100-nm NPs did not travel far from the injection site. Further investigation by Thomas *et al*. compared ipsilateral and contralateral i.d. injection of the 30-nm LN-draining poly(propylene sulfide) NPs conjugated with adjuvants for tumor treatment.[92]. Only ipsilaterally-injected NPs effectively traveled to the tumor dLN, whereas the contralateral injections traveled to non-tumor dLNs adjacent to the injection site. Furthermore, only stimulated tumor dLNs were able to slow tumor growth, highlighting the importance in optimizing injection site of NPs.

4.2.3 Factors to Consider in NP-size Lymph Node Targeting Studies—Though studies do not identify an exact optimal size, results suggest that the NP size for most efficient interstitial transport is between 20 and 50 nm and that larger particles only later reach the LNs by dendritic cell (DC) transport [93]. Discrepancies in the recognized size for LN targeting NPs can be attributed to a number of considerations. First, it is important to distinguish between the data that suggest LN uptake and those that suggest LN retention. The timescale of NP uptake and retention changes based on the study, ranging from minutes to days post-administration. This difference in temporal observation window obscures NP size-dependent effects. For example, LN imaging agents are transported quickly to the site to be imaged and must be cleared quickly to minimize toxicity [94]. NPs for this strategy,

therefore, would be measured on the order of minutes. However, for lymphatic drug and vaccine delivery, NPs display extended retention time to unload cargo within the LNs and may be detected on the order of hours to days. Thus characterization of NP targeting and/or retention should match the time points selected to characterize NP transport and biodistribution.

Second, the mesh size and composition of ECM and lymphatic flow characteristics likely vary by animal model, disease state, tissue type, and the age of the subject [95–97]. One area that has been relatively unexplored is relating ECM composition to NP transport, although work has characterized the effect of ECM composition on the transport of large molecules within normal and tumor microenvironments [84]. This may explain differing results observed when the same NPs were administered *via* different tissue-based injections methods (Figure 4b). This also poses an engineering challenge to generate NP preparations with sufficiently narrow size distribution in order to discern concrete NP size cutoffs for effective ECM- and LN-targeted transport.

4.2.4 Tissue-based Transport Phenomenon for Intravenously Injected NPs—

Although the analyses were derived from tissue-based injection studies, these considerations are also relevant to transport of i.v. injected NPs. Following extravasation from circulation, NPs migrating through extracellular space confront a similar set of barriers as those given through tissue-based injections. Even though 100-nm NPs may transport to the tissue site efficiently through the circulation system, they may not penetrate the tumor tissue easily. This has been noticed by Albanese *et al*. in a report with NPs of 40, 70, 110, and 150 nm [98]. The smaller NPs (40 and 70 nm) were observed within interstitial spaces, while larger NPs did not infiltrate tumor spheroids (Figure 4c). Furthermore, when 40-nm NPs were functionalized with a transferrin antibody, the accumulation and retention within the tumor spheroid increased nearly by 15-fold.

4.3 Mucosal Administration

Mucosal administration of NPs can be accomplished via pulmonary, vaginal, intranasal, or even oral administrations. Mucosal administration is beneficial due to a high tissue surface areas and thin membranes for fast absorption, tissue-specific targeting, and the relatively non-invasive nature [101, 102]. NP fate within these methods of administration is governed by several unique clearance mechanisms. Delivered through these routes, NPs first encounter the mucus layer and are absorbed by the gel layer and cleared either via mucosal transport or macrophage uptake. If NPs diffuse and disperse into the gel layer, they encounter a network of “sticky” gel molecules prior to reaching the epithelium and translocating to either the circulation or lymphatics [103]. Specifically for inhalation delivery, particles can induce coughing or sneezing whereby NPs may be eliminated through mechanical force.

It has been noted that decreasing particle size led to increasing NP distribution. For example, when comparing tissue distribution of orally administered 100, 500, 1000, and 3000 nm non-ionic polystyrene NPs in Peyer’s patches, villi, liver, LNs, and spleen of the rats, the highest levels of uptake were noticed for 100 and 500-nm particles; low level of tissue

uptake was found for the 1-μm particles, but none for the 3-μm particles [104], due to easier uptake of smaller by small intestine epithelium than larger NPs through para- and trans-epithelial transport [105]. Additionally, NP size also significantly influences NP diffusion through the mucus gel network similar to NP diffusion through the ECM; NP diffusion rate increases with decreasing size [106].

Though smaller NPs proved more effective in mucosal transport, recently studies have shown that decreasing NP size may not be the only factor affecting delivery efficiency. When pluronic-stabilized PPS NPs particles were administered intranasally with ovalbumin conjugated to the NPs, the larger 200-nm NPs activated the immune system more robustly than the 30-nm NPs [107]. This was shown both *in vitro* through stimulation of $CD4^+$ and $CD8^+$ T cells and *in vivo* with the generation of higher levels of antibody titers and polyfunctional T cells. This difference could relate to variations in NP surface characteristics compared to those used in previous studies. This surface effect has also been demonstrated recently by engineering “mucus penetrating particles” of sizes from 100 to 500 nm [108]. NPs coated with a dense layer of PEG showed low mucus retention compared to uncoated NPs. The coated NPs exhibited an increased diffusion rate; and small changes in PEG density and PEG MW resulted in several hundred fold differences in mucosal transport rate [109]. The pluronic-stabilized PPS NPs could be stabilized in a similar manner by the PEGylated corona, which allows for efficient NP transport. Therefore, in these delivery cases, size-dependent delivery efficiency of NPs should be considered together with the surface characteristics of NPs.

5. Size-shifting Particles

Just as many NP formulations using “smart” payload-release mechanism based on cleavage of labile bonds triggered by an environmental cue, NP size may also be tuned by environmental stimuli. For example, NPs have been induced to swell *in vivo* in response to a change in pH, heat, and light [110]. The swelling property has been used for endosomal escape and enhanced clearance upon NP delivery [111, 112]. This could potentially be used for size-specific transport properties, where smaller NP-specific transport properties are utilized and then swell in response to stimuli to become immobile at a specific tissue site. To the contrary, strategies have been designed to degrade larger NPs and release smaller NPs at the site of delivery by enzymes. Wong *et al*. developed 100-nm crosslinked gelatin NPs that contained 10-nm quantum dots, and showed that gelatin NPs were delivered to tumor site by the EPR effect and then gradually degraded by proteases within the tumor microenvironment, allowing smaller quantum dot NPs to penetrate deeper into the tumor tissue [113].

NP superstructures can be devised by linking NPs together. This can be used to exploit a larger NP size-related biodistribution properties, later cleaving into smaller NP satellites that use a unique smaller NP-related biodistribution pattern to target specific tissue locations. In one recent example, Chou *et al*. used specific DNA sequences to link 3 – 5 nm gold NPs to each other yielding larger NPs of about 100 nm [114]. These superstructures enabled a higher degree of tumor accumulation and retention; but can be cleaved to release the smaller NP components with good clearance by the kidney. An additional application involves the

encapsulation of NPs within larger MPs. One example uses microparticles as a carrier system for increased stability within a dry-powder inhaler administration. The microparticles quickly biodegrade, releasing NPs with improved biodistribution and penetration characteristics than a microparticle system [115].

Size-shifting NPs can be used to better understand the biodistribution and physiological effects of various NP aggregates and sizes, and also enable a variety of new targeting strategies. For example, a combination of the use of smaller NPs may provide quick and immediate transport and treatment, after which larger NPs could provide a depot effect for sustained drug release. Smart NPs, size-shifting NPs, and intelligent use of different NP size-dependent properties will help to develop more sophisticated and functional NP therapeutics.

6. Conclusion

The field of NP delivery has advanced significantly in identifying key physical and biochemical properties for engineering efficient functional carriers. The critical role of NP size on the delivery efficiency and function has been increasingly recognized for different applications. New methods for production of polymer NPs with a controlled and narrow size distribution are being developed. With improved control over size, structure, and biophysical properties of the NPs, their effect on molecular, cellular, and tissue interactions can be investigated at greater levels of details. Studies highlighted here illustrate size-dependent properties of NPs and their physiological fate, and demonstrate how these characteristics may be applied in various NP targeting strategies. To accurately describe the impact of NP size, confounding variables such as the “contextual size” of NPs need to be characterized in the development of NPs and analysis of the delivery results. Furthermore, biologically relevant *in vitro* assays, standardized *in vivo* experiments, quantifiable biodistribution NP statistics, and assessment in larger animal models are needed to fully characterize NP size effect. This will in turn spawn discoveries of other NP parameters important for biological fate such as shape [116]. As NP-size related physiological effects are understood better, engineering more efficient drug/vaccine delivery systems and imaging modalities will be possible, therefore accelerating the translation from laboratories to the clinic in diagnosis and treatment of various diseases.

Acknowledgements

This work was partially supported by the U.S. National Institute of Biomedical Imaging and Bioengineering (R01EB018358-01A1 and R21EB015152). J.W.H. acknowledges the support from the National Science Foundation Graduate Fellowship (DGE–1232825). Cell and protein corona images were reproduced under a Creative Commons License from Servier Medical Art (http://www.servier.com/Powerpoint-image-bank).

List of Abbreviations and Acronyms

CIJ	confined impinging jet
CPT	camptothecin
dLN	draining lymph node

ECM	extracellular matrix
EPR	enhanced permeability and retention
FNP	flash nanoprecipitation
i.d.	intradermal
i.v.	intravenous
LbL	layer-by-layer
LN	lymph node
MIVM	multi-inlet vortex mixer
MPS	mononuclear phagocyte system
NP	nanoparticle
PDI	polydispersity index
PEG	polyethylene glycol
PEG-*b*-PBLG	polyethylene glycol-*b*-poly(γ-benzyl L-glutamate)
PEI	polyethylenimine
PEG-*b*-PLGA	polyethylene glycol-*b*-poly(lactic-*co*-glycolic acid)
PPS	polypropylene sulfide
pTRAIL	TNF-related apoptosis including ligand
s.c.	subcutaneous
siRNA	small interfering RNA

References

1. Adjei IM, Peetla C, Labhasetwar V. Heterogeneity in nanoparticles influences biodistribution and targeting. Nanomedicine. 2014; 9:267–278. [PubMed: 23799984]
2. Wu L, Zhang J, Watanabe W. Physical and chemical stability of drug nanoparticles. Adv. Drug Deliv. Rev. 2011; 63:456–469. [PubMed: 21315781]
3. Shang L, Nienhaus K, Nienhaus GU. Engineered nanoparticles interacting with cells: size matters. J. Nanobiotechnology. 2014; 12:5. [PubMed: 24491160]
4. Cho EJ, Holback H, Liu KC, Abouelmagd SA, Park J, Yeo Y. Nanoparticle characterization: state of the art, challenges, and emerging technologies. Mol. Pharm. 2013; 10:2093–2110. [PubMed: 23461379]
5. Grzelczak M, Vermant J, Furst EM, Liz-Marzan LM. Directed self-assembly of nanoparticles. ACS Nano. 2010; 4:3591–3605. [PubMed: 20568710]
6. Rybtchinski B. Adaptive supramolecular nanomaterials based on strong noncovalent interactions. ACS Nano. 2011; 5:6791–6818. [PubMed: 21870803]
7. Ding J, Chen L, Xiao C, Chen L, Zhuang X, Chen X. Noncovalent interaction-assisted polymeric micelles for controlled drug delivery. Chem. Commun. 2014; 50:11274–11290.
8. Mendes AC, Baran ET, Reis RL, Azevedo HS. Self-assembly in nature: using the principles of nature to create complex nanobiomaterials. Wiley Interdiscip. Rev. Nanomed. Nanobiotechnol. 2013; 5:582–612. [PubMed: 23929805]

9. Hayward RC, Pochan DJ. Tailored assemblies of block copolymers in solution: it is all about the process. Macromolecules. 2010; 43:3577–3584.
10. Chan HK, Kwok PCL. Production methods for nanodrug particles using the bottom-up approach. Adv. Drug Deliv. Rev. 2011; 63:406–416. [PubMed: 21457742]
11. Anton N, Benoit J-P, Saulnier P. Design and production of nanoparticles formulated from nano-emulsion templates—a review. J. Control. Release. 2008; 128:185–199. [PubMed: 18374443]
12. Rao JP, Geckeler KE. Polymer nanoparticles: Preparation techniques and size-control parameters. Prog. Polym. Sci. 2011; 36:887–913.
13. Squires TM, Quake SR. Microfluidics: Fluid physics at the nanoliter scale. Rev. Mod. Phys. 2005; 77:977–1026.
14. Rhee M, Valencia PM, Rodriguez MI, Langer R, Farokhzad OC, Karnik R. Synthesis of size-tunable polymeric nanoparticles enabled by 3D hydrodynamic flow focusing in single-layer microchannels. Adv. Mater. 2011; 23:H79–H83. [PubMed: 21433105]
15. Valencia PM, Farokhzad OC, Karnik R, Langer R. Microfluidic technologies for accelerating the clinical translation of nanoparticles. Nat. Nanotechnol. 2012; 7:623–629. [PubMed: 23042546]
16. Rhee M, Valencia PM, Rodriguez MI, Langer R, Farokhzad OC, Karnik R. Synthesis of size-tunable polymeric nanoparticles enabled by 3D hydrodynamic flow focusing in single-layer microchannels. Adv. Mater. 2011; 23:H79–H83. [PubMed: 21433105]
17. Karnik R, Gu F, Basto P, Cannizzaro C, Dean L, Kyei-Manu W, Langer R, Farokhzad OC. Microfluidic platform for controlled synthesis of polymeric nanoparticles. Nano Lett. 2008; 8:2906–2912. [PubMed: 18656990]
18. Valencia PM, Pridgen EM, Perea B, Gadde S, Sweeney C, Kantoff PW, Bander NH, Lippard SJ, Langer R, Karnik R, Farokhzad OC. Synergistic cytotoxicity of irinotecan and cisplatin in dual-drug targeted polymeric nanoparticles. Nanomedicine. 2013; 8:687–698. [PubMed: 23075285]
19. Kolishetti N, Dhar S, Valencia PM, Lin LQ, Karnik R, Lippard SJ, Langer R, Farokhzad OC. Engineering of self-assembled nanoparticle platform for precisely controlled combination drug therapy. Proc. Natl. Acad. Sci. U.S.A. 2010; 107:17939–17944. [PubMed: 20921363]
20. Valencia PM, Pridgen EM, Rhee M, Langer R, Farokhzad OC, Karnik R. Microfluidic Platform for combinatorial synthesis and optimization of targeted nanoparticles for cancer therapy. ACS Nano. 2013; 7:10671–10680. [PubMed: 24215426]
21. Wang H, Liu K, Chen KJ, Lu YJ, Wang ST, Lin WY, Guo F, Kamei KI, Chen YC, Ohashi M, Wang MW, Garcia MA, Zhao XZ, Shen CKF, Tseng HR. A rapid pathway toward a superb gene delivery system: programming structural and functional diversity into a supramolecular nanoparticle library. ACS Nano. 2010; 4:6235–6243. [PubMed: 20925389]
22. Karnik R, Gu F, Basto P, Cannizzaro C, Dean L, Kyei-Manu W, Langer R, Farokhzad OC. Microfluidic platform for controlled synthesis of polymeric nanoparticles. Nano Lett. 2008; 8:2906–2912. [PubMed: 18656990]
23. Kolishetti N, Dhar S, Valencia PM, Lin LQ, Karnik R, Lippard SJ, Langer R, Farokhzad OC. Engineering of self-assembled nanoparticle platform for precisely controlled combination drug therapy. Proc. Natl. Acad. Sci. U.S.A. 2010; 107:17939–17944. [PubMed: 20921363]
24. Xu JH, Li SW, Tostado C, Lan WJ, Luo GS. Preparation of monodispersed chitosan microspheres and in situ encapsulation of BSA in a co-axial microfluidic device. Biomed. Microdevices. 2009; 11:243–249. [PubMed: 18810642]
25. Rolland JP, Van Dam RM, Schorzman DA, Quake SR, DeSimone JM. Solvent-resistant photocurable "liquid teflon" for microfluidic device fabrication. J. Am. Chem. Soc. 2004; 126:2322–2323. [PubMed: 14982433]
26. Liu DF, Cito S, Zhang YZ, Wang CF, Sikanen TM, Santos HA. A versatile and robust microfluidic platform toward high throughput synthesis of homogeneous nanoparticles with tunable properties. Adv. Mater. 2015; 27:2298–2304. [PubMed: 25684077]
27. Utada AS, Lorenceau E, Link DR, Kaplan PD, Stone HA, Weitz DA. Monodisperse double emulsions generated from a microcapillary device. Science. 2005; 308:537–541. [PubMed: 15845850]

28. Nicolas J, Mura S, Brambilla D, Mackiewicz N, Couvreur P. Design, functionalization strategies and biomedical applications of targeted biodegradable/biocompatible polymer-based nanocarriers for drug delivery. Chem. Soc. Rev. 2013; 42:1147–1235. [PubMed: 23238558]
29. Deng ZJ, Morton SW, Ben-Akiva E, Dreaden EC, Shopsowitz KE, Hammond PT. Layer-by-layer nanoparticles for systemic codelivery of an anticancer drug and siRNA for potential triple-negative breast cancer treatment. ACS Nano. 2013; 7:9571–9584. [PubMed: 24144228]
30. Ediriwickrema A, Zhou J, Deng Y, Saltzman WM. Multi-layered nanoparticles for combination gene and drug delivery to tumors. Biomaterials. 2014; 35:9343–9354. [PubMed: 25112935]
31. Morton SW, Herlihy KP, Shopsowitz KE, Deng ZJ, Chu KS, Bowerman CJ, DeSimone JM, Hammond PT. Scalable manufacture of built-to-order nanomedicine: spray-assisted layer-by-layer functionalization of PRINT nanoparticles. Adv. Mater. 2013; 25:4707–4713. [PubMed: 23813892]
32. Richardson JJ, Ejima H, Lorcher SL, Liang K, Senn P, Cui JW, Caruso F. Preparation of nano- and microcapsules by electrophoretic polymer assembly. Angew. Chem. Int. Ed. Engl. 2013; 52:6455–6458. [PubMed: 23657949]
33. Suma T, Miyata K, Anraku Y, Watanabe S, Christie RJ, Takemoto H, Shioyama M, Gouda N, Ishii T, Nishiyama N, Kataoka K. Smart multilayered assembly for biocompatible siRNA delivery featuring dissolvable silica, endosome-disrupting polycation, and detachable PEG. ACS Nano. 2012; 6:6693–6705. [PubMed: 22835034]
34. Akbulut M, Ginart P, Gindy ME, Theriault C, Chin KH, Soboyejo W, Prud'homme RK. Generic method of preparing multifunctional fluorescent nanoparticles using flash nanoprecipitation. Adv. Funct. Mater. 2009; 19:718–725.
35. Budijono SJ, Shan JN, Yao N, Miura Y, Hoye T, Austin RH, Ju YG, Prud'homme RK. Synthesis of stable block-copolymer-protected NaYF4:Yb3+Er3+ up-converting phosphor nanoparticles. Chem. Mater. 2010; 22:311–318.
36. Chen T, D'Addio SM, Kennedy MT, Swietlow A, Kevrekidis IG, Panagiotopoulos AZ, Prud'homme RK. Protected peptide nanoparticles: experiments and brownian dynamics simulations of the energetics of assembly. Nano Lett. 2009; 9:2218–2222. [PubMed: 19413305]
37. D'Addio SM, Baldassano S, Shi L, Cheung LL, Adamson DH, Bruzek M, Anthony JE, Laskin DL, Sinko PJ, Prud'homme RK. Optimization of cell receptor-specific targeting through multivalent surface decoration of polymeric nanocarriers. J. Control. Release. 2013; 168:41–49. [PubMed: 23419950]
38. D'Addio SM, Prud'homme RK. Controlling drug nanoparticle formation by rapid precipitation. Adv. Drug Deliv. Rev. 2011; 63:417–426. [PubMed: 21565233]
39. Gindy ME, Ji SX, Hoye TR, Panagiotopoulos AZ, Prud'homme RK. Preparation of Poly(ethylene glycol) protected nanoparticles with variable bioconjugate ligand density. Biomacromolecules. 2008; 9:2705–2711. [PubMed: 18759476]
40. Johnson BK, Prud'homme RK. Flash NanoPrecipitation of organic actives and block copolymers using a confined impinging jets mixer. Aust. J. Chem. 2003; 56:1021–1024.
41. Luo HY, Santos JL, Herrera-Alonso M. Toroidal structures from brush amphiphiles. Chem. Commun. 2014; 50:536–538.
42. Shan JN, Budijono SJ, Hu GH, Yao N, Kang YB, Ju YG, Prud'homme RK. Pegylated composite nanoparticles containing upconverting phosphors and meso-tetraphenyl porphine (TPP) for photodynamic therapy. Adv. Funct. Mater. 2011; 21:2488–2495.
43. Shen H, Hong SY, Prud'homme RK, Liu Y. Self-assembling process of flash nanoprecipitation in a multi-inlet vortex mixer to produce drug-loaded polymeric nanoparticles. J. Nanopart. Res. 2011; 13:4109–4120.
44. York AW, Zablocki KR, Lewis DR, Gu L, Uhrich KE, Prud'homme RK, Moghe PV. Kinetically assembled nanoparticles of bioactive macromolecules exhibit enhanced stability and cell-targeted biological efficacy. Adv. Mater. 2012; 24:733–739. [PubMed: 22223224]
45. Timko BP, Whitehead K, Gao W, Kohane DS, Farokhzad O, Anderson D, Langer R. Advances in drug delivery. Annu. Rev. Mater. Res. 2011; 41:1–20.
46. Chu KS, Schorzman AN, Finniss MC, Bowerman CJ, Peng L, Luft JC, Madden AJ, Wang AZ, Zamboni WC, DeSimone JM. Nanoparticle drug loading as a design parameter to improve

docetaxel pharmacokinetics and efficacy. Biomaterials. 2013; 34:8424–8429. [PubMed: 23899444]

47. Dunn SS, Tian SM, Blake S, Wang J, Galloway AL, Murphy A, Pohlhaus PD, Rolland JP, Napier ME, DeSimone JM. Reductively responsive siRNA-conjugated hydrogel nanoparticles for gene silencing. J. Am. Chem. Soc. 2012; 134:7423–7430. [PubMed: 22475061]
48. Rolland JP, Maynor BW, Euliss LE, Exner AE, Denison GM, DeSimone JM. Direct fabrication and harvesting of monodisperse, shape-specific nanobiomaterials. J. Am. Chem. Soc. 2005; 127:10096–10100. [PubMed: 16011375]
49. Xu J, Luft JC, Yi XW, Tian SM, Owens G, Wang J, Johnson A, Berglund P, Smith J, Napier ME, DeSimone JM. RNA replicon delivery via lipid-complexed PRINT protein particles. Mol. Pharm. 2013; 10:3366–3374. [PubMed: 23924216]
50. Russ B, Liu Y, Prud'homme RK. Optimized descriptive model for micromixing in a vortex mixer. Chem. Eng. Commun. 2010; 197:1068–1075.
51. Lee MY, Park SJ, Park K, Kim KS, Lee H, Hahn SK. Target-specific gene silencing of layer-by-layer assembled gold-cysteamine/siRNA/PEI/HA nanocomplex. ACS Nano. 2011; 5:6138–6147. [PubMed: 21739990]
52. Bjornmalm M, Roozmand A, Noi KF, Guo JL, Cui JW, Richardson JJ, Caruso F. Flow-based assembly of layer-by-layer capsules through tangential flow filtration. Langmuir. 2015; 31:9054–9060. [PubMed: 26267807]
53. Rabinow BE. Nanosuspensions in drug delivery. Nat. Rev. Drug Discov. 2004; 3:785–796. [PubMed: 15340388]
54. Nel AE, Mädler L, Velegol D, Xia T, Hoek EM, Somasundaran P, Klaessig F, Castranova V, Thompson M. Understanding biophysicochemical interactions at the nano-bio interface. Nat. Mater. 2009; 8:543–557. [PubMed: 19525947]
55. Min Y, Akbulut M, Kristiansen K, Golan Y, Israelachvili J. The role of interparticle and external forces in nanoparticle assembly. Nat. Mater. 2008; 7:527–538. [PubMed: 18574482]
56. Dunne M, Corrigan O, Ramtoola Z. Influence of particle size and dissolution conditions on the degradation properties of polylactide-co-glycolide particles. Biomaterials. 2000; 21:1659–1668. [PubMed: 10905407]
57. Tenzer S, Docter D, Kuharev J, Musyanovych A, Fetz V, Hecht R, Schlenk F, Fischer D, Kiouptsi K, Reinhardt C. Rapid formation of plasma protein corona critically affects nanoparticle pathophysiology. Nat. Nanotechnol. 2013; 8:772–781. [PubMed: 24056901]
58. Lundqvist M, Stigler J, Elia G, Lynch I, Cedervall T, Dawson KA. Nanoparticle size and surface properties determine the protein corona with possible implications for biological impacts. Proc. Natl. Acad. Sci. U.S.A. 2008; 105:14265–14270. [PubMed: 18809927]
59. Walkey CD, Olsen JB, Guo H, Emili A, Chan WC. Nanoparticle size and surface chemistry determine serum protein adsorption and macrophage uptake. J. Am. Chem. Soc. 2012; 134:2139–2147. [PubMed: 22191645]
60. Simpson J, Miller R, Spittle M. Liposomal doxorubicin for treatment of AIDS-related Kaposi's sarcoma. Clin. Oncol. 1993; 5:372–374.
61. Riley T, Stolnik S, Heald C, Xiong C, Garnett M, Illum L, Davis S, Purkiss S, Barlow R, Gellert P. Physicochemical evaluation of nanoparticles assembled from poly (lactic acid)-poly (ethylene glycol)(PLA-PEG) block copolymers as drug delivery vehicles. Langmuir. 2001; 17:3168–3174.
62. Behzadi S, Serpooshan V, Sakhtianchi R, Müller B, Landfester K, Crespy D, Mahmoudi M. Protein corona change the drug release profile of nanocarriers: the "overlooked" factor at the nanobio interface. Colloids Surf. B Biointerfaces. 2014; 123:143–149. [PubMed: 25262409]
63. Swami A, Reagan MR, Basto P, Mishima Y, Kamaly N, Glavey S, Zhang S, Moschetta M, Seevaratnam D, Zhang Y. Engineered nanomedicine for myeloma and bone microenvironment targeting. Proc. Natl. Acad. Sci. U.S.A. 2014 201401337.
64. Xia B, Zhang W, Shi J, Xiao S-j. Engineered stealth porous silicon nanoparticles via surface encapsulation of bovine serum albumin for prolonging blood circulation in vivo. ACS Appl. Mater. Interfaces. 2013; 5:11718–11724. [PubMed: 24138109]
65. Salvati A, Pitek AS, Monopoli MP, Prapainop K, Bombelli FB, Hristov DR, Kelly PM, Åberg C, Mahon E, Dawson KA. Transferrin-functionalized nanoparticles lose their targeting capabilities

when a biomolecule corona adsorbs on the surface. Nat. Nanotechnol. 2013; 8:137–143. [PubMed: 23334168]

66. Moghimi SM, Hawley AE, Christy NM, Gray T, Illum L, Davis SS. Surface engineered nanospheres with enhanced drainage into lymphatics and uptake by macrophages of the regional lymph nodes. FEBS Lett. 1994; 344:25–30. [PubMed: 8181558]
67. Rodriguez PL, Harada T, Christian DA, Pantano DA, Tsai RK, Discher DE. Minimal" Self" peptides that inhibit phagocytic clearance and enhance delivery of nanoparticles. Science. 2013; 339:971–975. [PubMed: 23430657]
68. Hu C-MJ, Zhang L, Aryal S, Cheung C, Fang RH, Zhang L. Erythrocyte membrane-camouflaged polymeric nanoparticles as a biomimetic delivery platform. Proc. Natl. Acad. Sci. U.S.A. 2011; 108:10980–10985. [PubMed: 21690347]
69. Allen C, Maysinger D, Eisenberg A. Nano-engineering block copolymer aggregates for drug delivery. Colloids Surf. B Biointerfaces. 1999; 16:3–27.
70. Liu H, Moynihan KD, Zheng Y, Szeto GL, Li AV, Huang B, Van Egeren DS, Park C, Irvine DJ. Structure-based programming of lymph-node targeting in molecular vaccines. Nature. 2014; 507:519–522. [PubMed: 24531764]
71. Tomalia DA. In quest of a systematic framework for unifying and defining nanoscience. J. Nanopart. Res. 2009; 11:1251–1310. [PubMed: 21170133]
72. Longmire MR, Ogawa M, Choyke PL, Kobayashi H. Biologically optimized nanosized molecules and particles: more than just size. Bioconjugate Chem. 2011; 22:993–1000.
73. Ogawa M, Regino CAS, Marcelino B, Williams M, Kosaka N, Bryant LH, Choyke PL, Kobayashi H. New nanosized biocompatible MR contrast agents based on lysine-dendri-graft macromolecules. Bioconjugate Chem. 2010; 21:955–960.
74. Anselmo AC, Mitragotri S. An overview of clinical and commercial impact of drug delivery systems. J. Control. Release. 2014; 190:15–28. [PubMed: 24747160]
75. Prausnitz MR, Langer R. Transdermal drug delivery. Nat. Biotechnol. 2008; 26:1261–1268. [PubMed: 18997767]
76. Zhang X-D, Wu H-Y, Wu D, Wang Y-Y, Chang J-H, Zhai Z-B, Meng A-M, Liu P-X, Zhang L-A, Fan F-Y. Toxicologic effects of gold nanoparticles in vivo by different administration routes. Int. J. Nanomedicine. 2010; 5:771–781. [PubMed: 21042423]
77. Choi HS, Liu W, Misra P, Tanaka E, Zimmer JP, Ipe BI, Bawendi MG, Frangioni JV. Renal clearance of quantum dots. Nat. Biotechnol. 2007; 25:1165–1170. [PubMed: 17891134]
78. Moghimi SM, Hunter AC, Murray JC. Long-circulating and target-specific nanoparticles: theory to practice. Pharmacol. Rev. 2001; 53:283–318. [PubMed: 11356986]
79. Jain RK, Stylianopoulos T. Delivering nanomedicine to solid tumors. Nat. Rev. Clin. Oncol. 2010; 7:653–664. [PubMed: 20838415]
80. Jhaveri AM, Torchilin VP. Multifunctional polymeric micelles for delivery of drugs and siRNA. Front. Pharmacol. 2014; 5:77. [PubMed: 24795633]
81. Wang J, Wu W, Zhang Y, Wang X, Qian H, Liu B, Jiang X. The combined effects of size and surface chemistry on the accumulation of boronic acid-rich protein nanoparticles in tumors. Biomaterials. 2014; 35:866–878. [PubMed: 24157313]
82. Cabral H, Makino J, Matsumoto Y, Mi P, Wu H, Nomoto T, Toh K, Yamada N, Higuchi Y, Konishi S. Systemic targeting of lymph node metastasis through the blood vascular system by using size-controlled nanocarriers. ACS Nano. 2015; 9:4957–4967. [PubMed: 25880444]
83. Cabral H, Matsumoto Y, Mizuno K, Chen Q, Murakami M, Kimura M, Terada Y, Kano M, Miyazono K, Uesaka M. Accumulation of sub-100 nm polymeric micelles in poorly permeable tumours depends on size. Nat. Nanotechnol. 2011; 6:815–823. [PubMed: 22020122]
84. Jain RK. Transport of molecules in the tumor interstitium: a review. Cancer Res. 1987; 47:3039–3051. [PubMed: 3555767]
85. Fifis T, Gamvrellis A, Crimeen-Irwin B, Pietersz GA, Li J, Mottram PL, McKenzie IF, Plebanski M. Size-dependent immunogenicity: therapeutic and protective properties of nano-vaccines against tumors. J. Immunol. 2004; 173:3148–3154. [PubMed: 15322175]

86. Rao DA, Forrest ML, Alani AWG, Kwon GS, Robinson JR. Biodegradable PLGA based nanoparticles for sustained regional lymphatic drug delivery. J. Pharm. Sci. 2010; 99:2018–2031. [PubMed: 19902520]

87. Oussoren C, Zuidema J, Crommelin DJA, Storm G. Lymphatic uptake and biodistribution of liposomes after subcutaneous injection.: II. Influence of liposomal size, lipid composition and lipid dose. Biochim. Biophys. Acta. 1997; 1328:261–272. [PubMed: 9315622]

88. Khullar OV, Griset AP, Gibbs-Strauss SL, Chirieac LR, Zubris KAV, Frangioni JV, Grinstaff MW, Colson YL. Nanoparticle migration and delivery of paclitaxel to regional lymph nodes in a large animal model. J. Am. Coll. Surg. 2012; 214:328–337. [PubMed: 22225645]

89. Zubris KAV, Khullar OV, Griset AP, Gibbs-Strauss S, Frangioni JV, Colson YL, Grinstaff MW. Ease of synthesis, controllable sizes, and in vivo large-animal-lymph migration of polymeric nanoparticles. ChemMedChem. 2010; 5:1435–1438. [PubMed: 20593440]

90. Reddy ST, Rehor A, Schmoekel HG, Hubbell JA, Swartz MA. In vivo targeting of dendritic cells in lymph nodes with poly(propylene sulfide) nanoparticles. J. Control. Release. 2006; 112:26–34. [PubMed: 16529839]

91. Reddy ST, van der Vlies AJ, Simeoni E, Angeli V, Randolph GJ, O'Neil CP, Lee LK, Swartz MA, Hubbell JA. Exploiting lymphatic transport and complement activation in nanoparticle vaccines. Nat. Biotechnol. 2007; 25:1159–1164. [PubMed: 17873867]

92. Thomas SN, Vokali E, Lund AW, Hubbell JA, Swartz MA. Targeting the tumor-draining lymph node with adjuvanted nanoparticles reshapes the anti-tumor immune response. Biomaterials. 2014; 35:814–824. [PubMed: 24144906]

93. Manolova V, Flace A, Bauer M, Schwarz K, Saudan P, Bachmann MF. Nanoparticles target distinct dendritic cell populations according to their size. Eur. J. Immunol. 2008; 38:1404–1413. [PubMed: 18389478]

94. Kim K-R, Lee Y-D, Lee T, Kim B-S, Kim S, Ahn D-R. Sentinel lymph node imaging by a fluorescently labeled DNA tetrahedron. Biomaterials. 2013; 34:5226–5235. [PubMed: 23587443]

95. Swartz MA, Hubbell JA, Reddy ST. Lymphatic drainage function and its immunological implications: From dendritic cell homing to vaccine design. Semin. Immunol. 2008; 20:147–156. [PubMed: 18201895]

96. Proulx ST, Luciani P, Christiansen A, Karaman S, Blum KS, Rinderknecht M, Leroux J-C, Detmar M. Use of a PEG-conjugated bright near-infrared dye for functional imaging of rerouting of tumor lymphatic drainage after sentinel lymph node metastasis. Biomaterials. 2013; 34:5128–5137. [PubMed: 23566803]

97. Hirakawa S, Detmar M, Karaman S. Lymphatics in nanophysiology. Adv. Drug Deliv. Rev. 2014; 74:12–18. [PubMed: 24524932]

98. Albanese A, Lam AK, Sykes EA, Rocheleau JV, Chan WC. Tumour-on-a-chip provides an optical window into nanoparticle tissue transport. Nat. Commun. 2013; 4:2718. [PubMed: 24177351]

99. Irvine DJ, Swartz MA, Szeto GL. Engineering synthetic vaccines using cues from natural immunity. Nat. Mater. 2013; 12:978–990. [PubMed: 24150416]

100. Mohanan D, Slütter B, Henriksen-Lacey M, Jiskoot W, Bouwstra JA, Perrie Y, Kündig TM, Gander B, Johansen P. Administration routes affect the quality of immune responses: A cross-sectional evaluation of particulate antigen-delivery systems. J. Control. Release. 2010; 147:342–349. [PubMed: 20727926]

101. Weber S, Zimmer A, Pardeike J. Solid lipid nanoparticles (SLN) and nanostructured lipid carriers (NLC) for pulmonary application: a review of the state of the art. Eur. J. Pharm. Biopharm. 2014; 86:7–22. [PubMed: 24007657]

102. Zhang J, Wu L, Chan H-K, Watanabe W. Formation, characterization, and fate of inhaled drug nanoparticles. Adv. Drug Deliv. Rev. 2011; 63:441–455. [PubMed: 21118707]

103. Ensign LM, Schneider C, Suk JS, Cone R, Hanes J. Mucus penetrating nanoparticles: biophysical tool and method of drug and gene delivery. Adv. Mater. 2012; 24:3887–3894. [PubMed: 22988559]

104. Jani P, Halbert G, Langridge J, Florence A. The uptake and translocation of latex nanospheres and microspheres after oral administration to rats. J. Pharm. Pharmacol. 1989; 41:809–812. [PubMed: 2576440]

105. Win KY, Feng S-S. Effects of particle size and surface coating on cellular uptake of polymeric nanoparticles for oral delivery of anticancer drugs. Biomaterials. 2005; 26:2713–2722. [PubMed: 15585275]

106. Norris DA, Puri N, Sinko PJ. The effect of physical barriers and properties on the oral absorption of particulates. Adv. Drug Deliv. Rev. 1998; 34:135–154. [PubMed: 10837675]

107. Stano A, Nembrini C, Swartz MA, Hubbell JA, Simeoni E. Nanoparticle size influences the magnitude and quality of mucosal immune responses after intranasal immunization. Vaccine. 2012; 30:7541–7546. [PubMed: 23103199]

108. Lai SK, O'Hanlon DE, Harrold S, Man ST, Wang Y-Y, Cone R, Hanes J. Rapid transport of large polymeric nanoparticles in fresh undiluted human mucus. Proc. Natl. Acad. Sci. U.S.A. 2007; 104:1482–1487. [PubMed: 17244708]

109. Wang YY, Lai SK, Suk JS, Pace A, Cone R, Hanes J. Addressing the PEG mucoadhesivity paradox to engineer nanoparticles that "lip"through the human mucus barrier. Angew. Chem. Int. Ed. Engl. 2008; 47:9726–9729. [PubMed: 18979480]

110. Yoo J-W, Doshi N, Mitragotri S. Adaptive micro and nanoparticles: temporal control over carrier properties to facilitate drug delivery. Adv. Drug Deliv. Rev. 2011; 63:1247–1256. [PubMed: 21605607]

111. Choi SH, Lee SH, Park TG. Temperature-sensitive pluronic/poly(ethylenimine) nanocapsules for thermally triggered disruption of intracellular endosomal compartment. Biomacromolecules. 2006; 7:1864–1870. [PubMed: 16768408]

112. Hu Y, Litwin T, Nagaraja AR, Kwong B, Katz J, Watson N, Irvine DJ. Cytosolic delivery of membrane-impermeable molecules in dendritic cells using pH-responsive core-shell nanoparticles. Nano Lett. 2007; 7:3056–3064. [PubMed: 17887715]

113. Wong C, Stylianopoulos T, Cui J, Martin J, Chauhan VP, Jiang W, Popović Z, Jain RK, Bawendi MG, Fukumura D. Multistage nanoparticle delivery system for deep penetration into tumor tissue. Proc. Natl. Acad. Sci. U.S.A. 2011; 108:2426–2431. [PubMed: 21245339]

114. Chou LY, Zagorovsky K, Chan WC. DNA assembly of nanoparticle superstructures for controlled biological delivery and elimination. Nat. Nanotechnol. 2014; 9:148–155. [PubMed: 24463361]

115. Sham JO-H, Zhang Y, Finlay WH, Roa WH, Löbenberg R. Formulation and characterization of spray-dried powders containing nanoparticles for aerosol delivery to the lung. Int. J. Pharm. 2004; 269:457–467. [PubMed: 14706257]

116. Williford J-M, Santos JL, Shyam R, Mao H-Q. Shape control in engineering of polymeric nanoparticles for therapeutic delivery. Biomater. Sci. 2015; 3:894–907. [PubMed: 26146550]

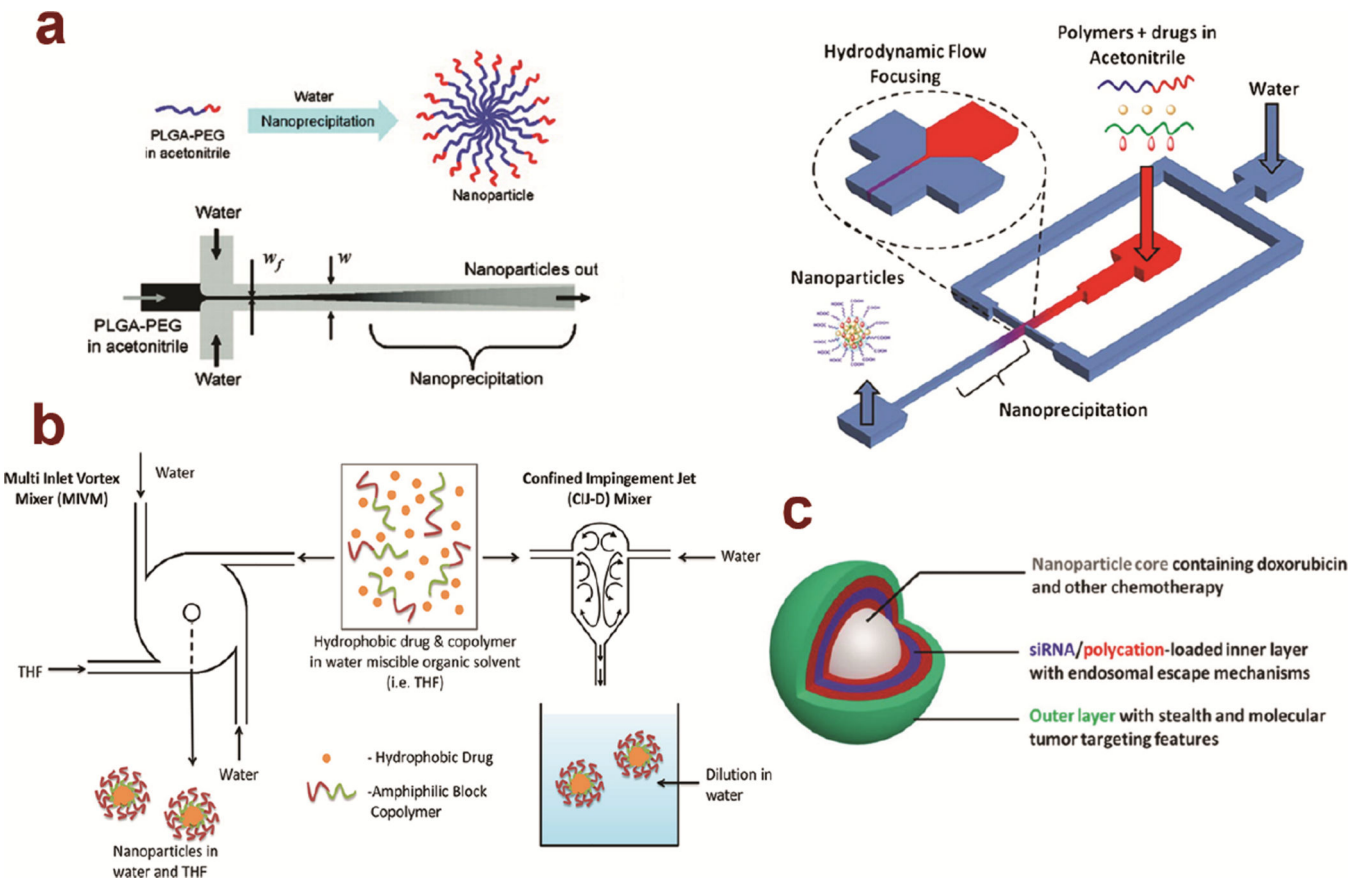

Figure 1. Methods have been developed for precise control of NP size

(a) Fabrication of polymer NPs containing anticancer drugs using a simple diffusion based continuous-flow microfluidic device (top left panel, adapted with permission from [17]. Copyright (2008) American Chemical Society) or a hydrodynamic flow focusing device (top right panel, adapted with permission from [19]. Copyright (2010) National Academy of Sciences of the USA). (b) Preparation of block copolymer stabilized-NPs using confined precipitation geometries of four (MIVM) or two (CIJ) impinging fluid streams. Reprinted from [38], copyright (2011), with permission from Elsevier. Hydrophobic solute and block copolymers are dissolved in a water miscible organic solvent and brought together with water into a confined space to generate NPs. The final concentration of organic solvent is <10%. (c) Schematic representation of NPs prepared using LbL method with controlled size and surface characteristics. Reprinted with permission from [29]. Copyright (2013) American Chemical Society. Sequential layers of oppositely charged macromolecules can be added to the NP core, allowing for the delivery of therapeutics, including DNA and RNA, and coating with an outer layer for long circulation and targeting capabilities.

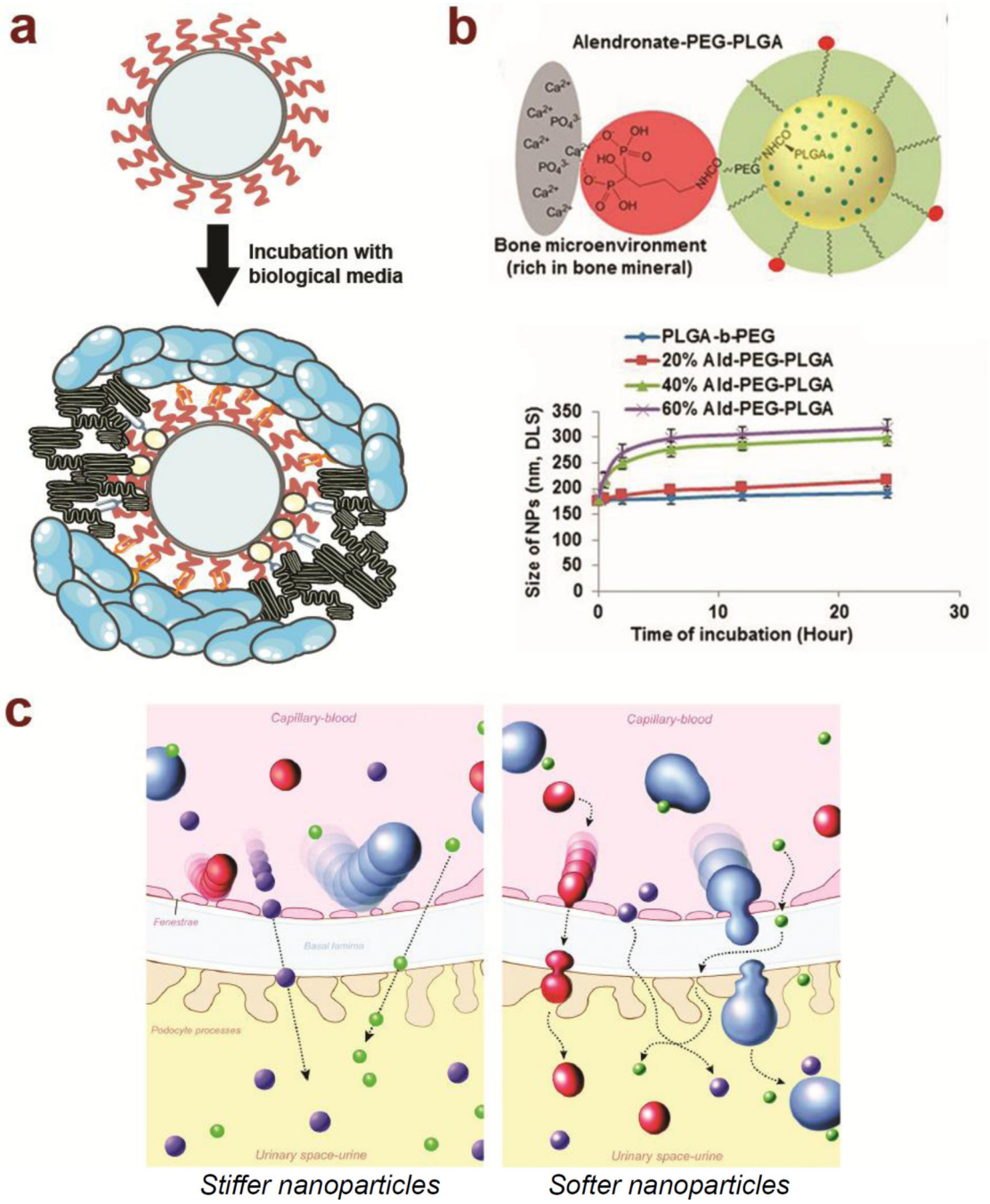

Figure 2. Environmental factors that influence contextual size of NPs

(a) NP surface characteristics after fabrication in PBS or water changes drastically upon incubation in biological media, such as serum. (b) Schematic representation of PLGA-PEG-alendronate NPs with various amounts of alendronate conjugated to the surface for bone targeting. NP size increases were observed after incubation in serum, particularly for high alendronate surface modification. Reprinted with permission from [63]. Copyright (2014) National Academy of Sciences of the USA. (c) NP rigidity influences the ability to be cleared by the kidney. For stiffer nanoparticles, only those smaller than pores in the

capillaries could be filtered. Softer and more flexible nanoparticles could deform through the capillary bed, allowing larger particles to be cleared. Reprinted with permission from [72]. Copyright (2011) American Chemical Society.

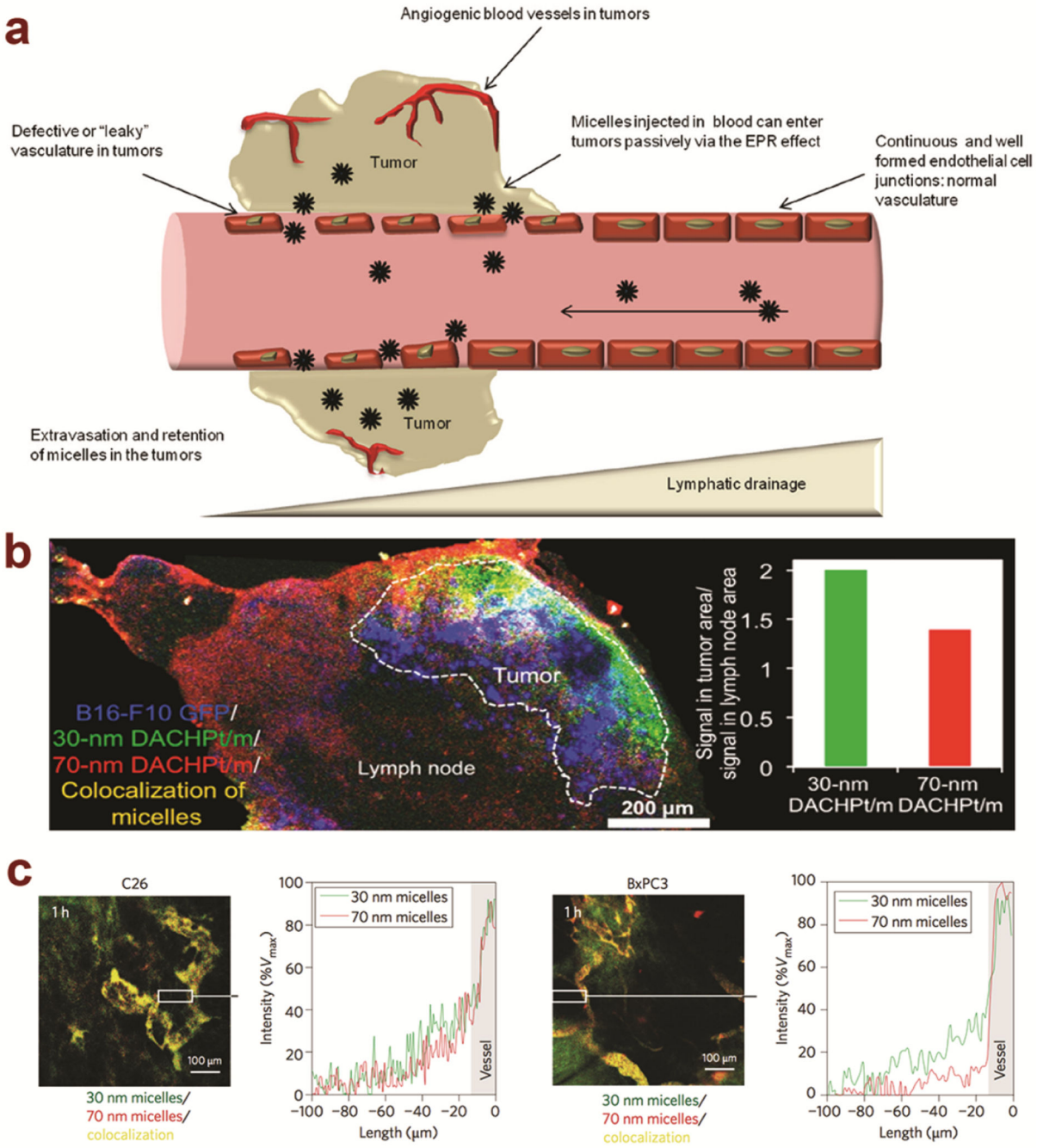

Figure 3. NP size influences tumor delivery via i.v. administration

(a) Schematic representation of the EPR effect for NP delivery to solid tumors through fenestrations in tumor-associated blood vessels. Reprinted with permission from [80]. (b) Fluorescent microscopy image of distribution of 30-nm (green) and 70-nm (red) polymeric micelles in metastatic LN 24 h after systemic injection of micelles. B16-F10 melanoma cells are shown in blue, and micelle co-localization is shown in yellow. Fluorescent intensity of micelles was quantified in both the metastatic region and normal region of the LN, and the ratio was plotted to compare the size-dependent distribution. Adapted with permission from

[82]. Copyright (2015) American Chemical Society. (c) Fluorescent microscopy images showing distribution of 30-nm (green) and 70-nm (red) micelles in C26 and BxPC3 tumors. Co-localization of micelles is shown in yellow. Graphs depict the fluorescent intensity of the two micelles in the white rectangle box, with the 0 – 10 μm region characterizing the distribution inside the blood vessel and the 10 – 100 μm region characterizing the distribution in the tumor tissue. Values are expressed as a maximum of the fluorescent intensity in the blood vessel region. Reprinted by permission from Macmillan Publishers Ltd: *Nature Nanotechnology* [83], copyright 2011.

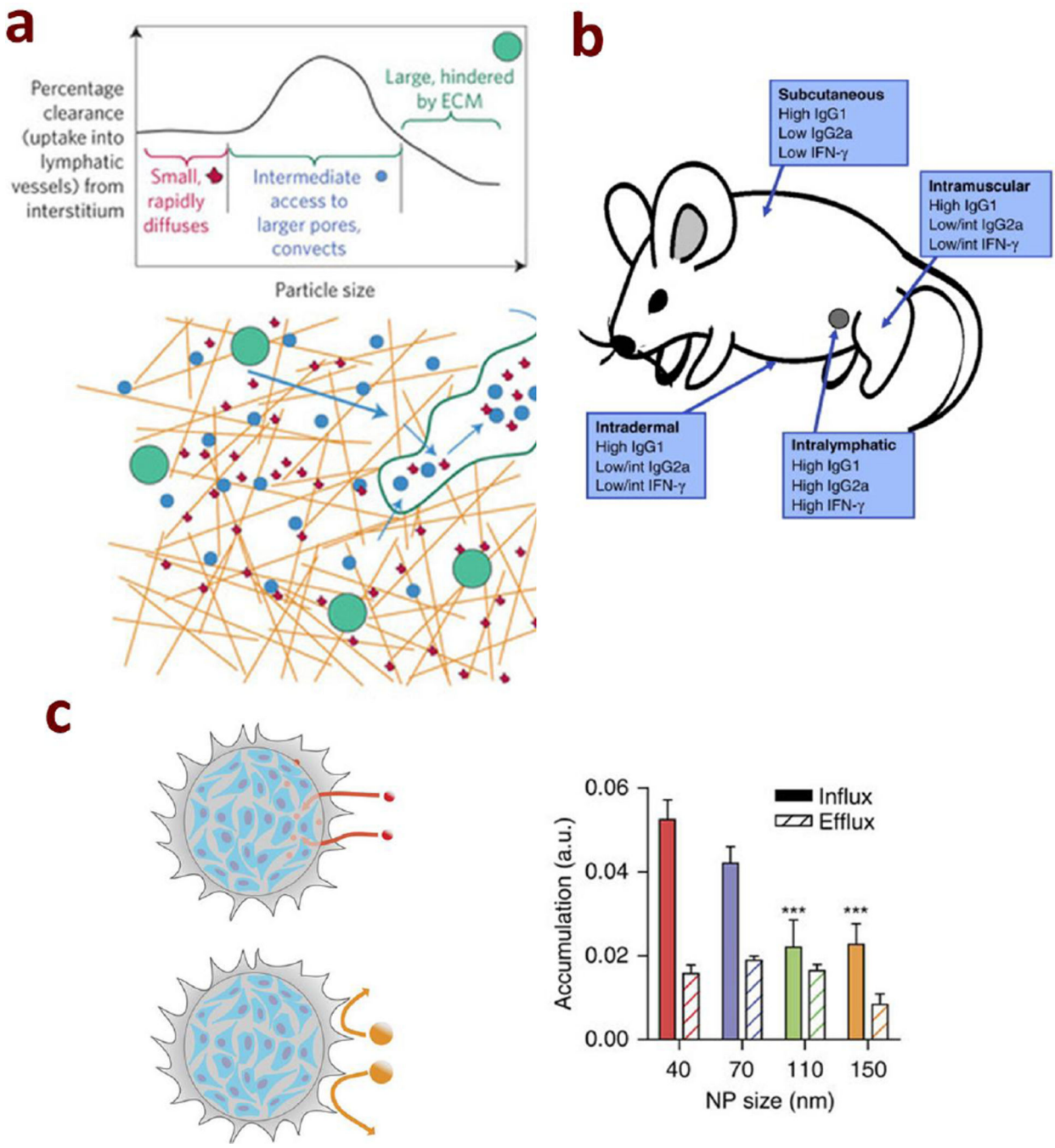

Figure 4. NP size affects tissue biodistribution in tissue-based injections

(a) Schematic illustration depicting transport of 1 – 100 nm NPs versus larger NP within fibrous ECM matrix highlighting increased ability of smaller NPs to navigate the ECM. Upon transport to LNs, size also significantly influences NP retention. Reprinted by permission from Macmillan Publishers Ltd: *Nature Materials* [99], copyright 2013. (b) Administration route influences the immune response of different sized NPs. Reprinted from [100], copyright (2010), with permission from Elsevier. (c) NPs encounter tissue ECM barriers to transport upon reaching target tissues and exhibit further NP size dependent

properties such as tumor accumulation. Reprinted by permission from Macmillan Publishers Ltd: *Nature Communications* [98], copyright 2013.

Table 1

Summary of methods for the preparation of polymer NPs with controlled sizes

Preparation Method		Unique Features	Polymeric Carrier	Cargos Packaged
Batch-mode preparation	Nanoprecipitation Emulsion/ Evaporation Dialysis [11, 12, 28]	• Does not require special apparatus or devices • Poor micromixing, leading to relatively low drug loading efficiency and capacity • Low uniformity in size and shape • High batch-to-batch variability • Challenging to scale up • Particles of well-defined size and shape (spheres, rods, cubes), high loading efficiency, time consuming process	Block copolymers, polyelectrolytes, polymer-drug conjugates	Small molecule drugs, nucleic acids, proteins, antibodies, contrast agents
	Layer-by-layer assembly [29–33]		Polyelectrolytes, proteins, hydrogen bond-forming polymers; Template needed	Small molecule drugs, nucleic acids, proteins, antibodies, contrast agents
Flow-based preparation	Flash Nanoprecipitation [34–44]	• Well-defined micromixing environment • High drug loading efficiency • High yield formulations with uniformity in size • Excellent control over particle size; • Continuous, low-cost, and scalable process	Block copolymer, homopolymers, polymer-sugar conjugates	Small molecule drugs, contrast agents, semiconducting polymers, gold NPs
	Microfluidic devices [16–20, 35, 45]	• Enables high-throughput screening of NPs • High reproducibility • Challenging to scale up	Block copolymers, polyelectrolytes	Small molecule drugs, nucleic acids, proteins, antibodies, contrast agents
Lithography-based preparation	PRINT [46–49]	• Particles of well-defined size and shape (spheres, rods, cubes) • Can be scaled up • Limited choice of cargos for loading	Polymers, proteins	Small molecule drugs, siRNA, contrast agents